Electromagnetic fields in ultra-peripheral relativistic heavy-ion collisions

Jie Zhao[1,2] · Jin-Hui Chen[1,2] · Xu-Guang Huang[1,2,3] · Yu-Gang Ma[1,2]

Abstract

Ultra-peripheral heavy-ion collisions (UPCs) offer unique opportunities to study processes under strong electromagnetic fields. In these collisions, highly charged fast-moving ions carry strong electromagnetic fields that can be effectively treated as photon fluxes. The exchange of photons can induce photonuclear and two-photon interactions and excite ions. This excitation of the ions results in Coulomb dissociation with the emission of photons, neutrons, and other particles. Additionally, the electromagnetic fields generated by the ions can be sufficiently strong to enforce mutual interactions between the two colliding ions. Consequently, the two colliding ions experience an electromagnetic force that pushes them in opposite directions, causing a back-to-back correlation in the emitted neutrons. Using a Monte Carlo simulation, we qualitatively demonstrate that the above electromagnetic effect is large enough to be observed in UPCs, which would provide a clear means to study strong electromagnetic fields and their effects.

Keywords Electromagnetic fields · Neutrons · Ultra-peripheral relativistic heavy-ion collisions (UPC)

✉ Jin-Hui Chen
chenjinhui@fudan.edu.cn

✉ Xu-Guang Huang
huangxuguang@fudan.edu.cn

Jie Zhao
jie_zhao@fudan.edu.cn

1 Key Laboratory of Nuclear Physics and Ion-beam Application (MOE), Institute of Modern Physics, Fudan University, Shanghai 200433, China

2 Shanghai Research Center for Theoretical Nuclear Physics, NSFC and Fudan University, Shanghai 200438, China

3 Physics Department and Center for Particle Physics and Field Theory, Fudan University, Shanghai 200438, China

1 Introduction

Over the past two decades, several novel phenomena associated with strong electromagnetic fields in hot quantum chromodynamics (QCD) have been proposed, such as the chiral magnetic effect (CME) [1–6]. Such strong electromagnetic fields are expected to be generated during relativistic heavy-ion collisions; however, they are extremely challenging to measure experimentally. Several attempts have been made to detect strong electromagnetic fields in heavy ion collisions [7–10]. However, electromagnetic processes are obscured by strong hadronic interactions when nuclei collide. Conversely, ultra-peripheral heavy-ion collisions (UPCs) offer a distinctive advantage in observing electromagnetic processes, as the impact parameters in these collisions are more than twice the nuclear radius, preventing hadronic interactions [11–13]. Therefore, UPCs provide a unique opportunity to study strong electromagnetic processes in relativistic heavy ion collisions [11, 14].

In UPCs, fast-moving heavy ions are accompanied by intense photon fluxes due to their large electric charges and strong Lorentz-contracted electromagnetic fields. These fields are sufficiently strong to induce photonuclear and photon–photon interactions [11–13]. Many interesting

results regarding particle production, including $e^+ + e^-$ and $\pi^+ + \pi^-$, and vector mesons, such as $\rho, \omega, J/\psi$ have been reported in UPCs [15–21]. Thus, it is natural to assume that these strong electromagnetic fields could likewise have visible impacts on collision dynamics through the electromagnetic force.

The most important region for Coulomb dissociation is the giant dipole resonance (GDRs) [22] around a few MeVs. The photon–nuclear interaction in UPCs has a large cross section to produce GDRs or excite nuclei to high-energy states [23, 24]. The GDRs typically decay by emitting photons and neutrons. The excitation energy of the GDRs is approximately 10–14 MeV for heavy nuclei and higher for lighter nuclei [23, 25–28]. The emitted neutrons have similar energies, which are considerably lower than the typical energy scales of relativistic heavy-ion collisions. Consequently, the emitted neutrons can be used to detect strong electromagnetic fields. In this study, we employed Monte (MC) simulations to demonstrate that the electromagnetic effect on neutron emission from Coulomb dissociation, primarily through GDRs decay, is sufficiently significant to be observed in UPCs. Our simulation incorporates the calculation of the strong electromagnetic field using Liénard-Wiechert potential, combined with neutron emission data from the existing experimental results and model simulations. Natural units $\hbar = c = 1$ are used in this study.

2 General idea

When two ions collide in the UPC, a strong electromagnetic field is generated. For instance, in a gold-gold (Au + Au) UPC with an impact parameter of $b = 20$ fm [29] and a center-of-mass energy of $\sqrt{s_{NN}} = 200$ GeV, as shown in Fig. 1, the electric and magnetic fields produced by one nucleus acting on another are approximately $eE \sim 0.2m_\pi^2$ and $eB \sim 0.2m_\pi^2$, respectively, [30, 31]. Electric and Lorentz forces would push the two colliding ions in opposite directions in the transverse plane. Assuming that the nuclei have no initial transverse moment, the velocity of each nucleon can be calculated using the following equation:

$$v_z^2 = 1 - \left(2m_N / \sqrt{s_{NN}}\right)^2, \tag{1}$$

where m_N denotes nucleon mass. At the RHIC and LHC energies, where v_z is very large, the nuclei are strongly Lorentz contracted and adopt a pancake-like shape. The effective collision time is estimated as $\Delta t = 2R/(\gamma v_z)$ [11], where R is the radius of the nucleus and $\gamma = 1/\sqrt{(1 - v_z^2)}$ is the Lorentz factor, which is approximately 107 for Au + Au collisions at $\sqrt{s_{NN}} = 200$ GeV. Hence, during the collision, the transverse momentum per nucleon due to the strong
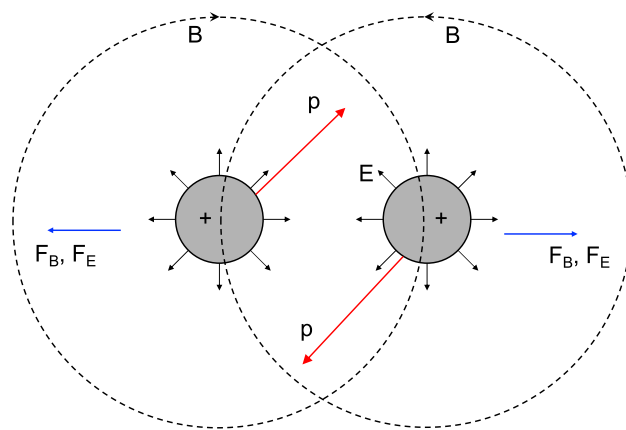
Fig. 1 (Color online) Schematic view of electromagnetic forces in an ultra-peripheral relativistic heavy-ion collision, where the impact parameter $b > 2R$ (R is the nuclear radius). Red arrows indicate the moving directions of the two colliding nuclei. The two fast-moving nuclei are highly charged (positively electric charged). The electric-field directions are indicated by the black solid arrows. The black-dashed lines show the magnetic-field directions. Both the electric and Lorentz forces push the two nuclei in opposite directions, as indicated by the blue arrows. The electromagnetic forces are strong enough to impact the emission of particles from the nuclei. For instance, the neutrons, emitted from the Coulomb dissociation of two colliding ions (such as the GDRs decay), will have a back-to-back correlation in the transverse plane

electromagnetic field is approximately 2 MeV by a rough estimate [$\Delta p = Z(eE + v_z eB)\Delta t/A \approx 0.4m_\pi^2 \times 0.12$ fm $\times 79/197 \sim 2$ MeV, with $Z = 79, A = 197$, and $R = 6.38$ fm for the Au nucleus].

However, the excitation energy of a typical GDRs is about 10–14 MeV for heavy nuclei [23]. Owing to the large GDR cross section in photonuclear interactions, the exchange of photons between two colliding nuclei in a UPC event has a high probability of exciting one or both ions into GDRs or even higher excitations. GDRs can decay by emitting a single neutron, whereas higher-excitation resonances can decay by emitting two or more neutrons [23, 32, 33]. These neutrons have low momenta, approximately ~ 10 MeV, comparable to the transverse momentum shift, Δp, induced by the electromagnetic force. Thus, strong electromagnetic fields may affect the momentum distribution of the emitted neutrons, such that their emission directions correlate with the direction of the impact parameter or the electromagnetic fields. Consequently, a back-to-back correlation may occur between the neutrons emitted from the two colliding nuclei. This provides a means of investigating strong electromagnetic fields in UPCs and offers a way to measure the direction of the impact parameter or electromagnetic field.

3 Electromagnetic fields

The electromagnetic fields can be calculated using the Liénard-Wiechert potentials, as described in Refs. [30, 34]. The electric and magnetic fields are expressed as follows:

$$
e\boldsymbol{E}(t,\boldsymbol{r}) = \frac{e^2}{4\pi} \sum_n Z_n \frac{\boldsymbol{R}_n - R_n \boldsymbol{v}_n}{(R_n - \boldsymbol{R}_n \cdot \boldsymbol{v}_n)^3}(1 - v_n^2),
$$
$$
e\boldsymbol{B}(t,\boldsymbol{r}) = \frac{e^2}{4\pi} \sum_n Z_n \frac{\boldsymbol{v}_n \times \boldsymbol{R}_n}{(R_n - \boldsymbol{R}_n \cdot \boldsymbol{v}_n)^3}(1 - v_n^2),
\tag{2}
$$

where Z_n denotes the charge number of the nth particle. Here, $\boldsymbol{R}_n = \boldsymbol{r} - \boldsymbol{r}_n$ represents the relative coordinates of the field point $\boldsymbol{r}$ to the location $\boldsymbol{r}_n$ of the nth particle with velocity $\boldsymbol{v}_n$ at retarded time $t_n = t - |\boldsymbol{r} - \boldsymbol{r}_n|$. Summations are performed for all protons in the nucleus.

For UPCs, around the collision time $t = 0$, Eq. (2) can be approximated as

$$
e\boldsymbol{E}_\perp(0,\boldsymbol{r}) \approx Z \frac{e^2}{4\pi} \frac{\sqrt{s_{NN}}}{2m_N} \frac{\boldsymbol{R}_\perp}{|\boldsymbol{R}_\perp|^3},
$$
$$
e\boldsymbol{B}_\perp(0,\boldsymbol{r}) \approx Z \frac{e^2}{4\pi} \frac{\sqrt{s_{NN}}}{2m_N} \frac{\boldsymbol{e}_z \times \boldsymbol{R}_\perp}{|\boldsymbol{R}_\perp|^3},
\tag{3}
$$

where $\boldsymbol{e}_z$ denotes the unit vector in $\pm z$ direction (depending on whether the source nucleus is the target or projectile nucleus), $\boldsymbol{R}_\perp$ denotes the transverse position of the center of the source nucleus, and Z denotes the total charge number of the source nucleus.

4 Toy model simulation

To obtain more quantitative results, MC simulations are performed. We parameterize the nucleon density distribution of the nucleus using the Woods–Saxon function [35]:

$$
\rho(r) = \frac{1}{1 + \exp[(r - R)/a]},
\tag{4}
$$

where $a = 0.54$ fm is the skin depth parameter, and $R = 6.38$ fm is the Au nucleus in this calculation. The electromagnetic fields are calculated using Eq. (3) [30, 31]. We obtained the momentum per nucleon induced by strong electric and Lorentz forces through the following integration:

$$
\Delta\boldsymbol{p}(b) = \int_{t=-\infty}^{t=+\infty} \boldsymbol{F}\mathrm{d}t = \int_{t=-\infty}^{t=+\infty} (q\boldsymbol{E} + q\boldsymbol{v} \times \boldsymbol{B})\mathrm{d}t,
\tag{5}
$$

where $q = Ze/A$ denotes the average charge per nucleon. Due to the Lorentz contraction, the longitudinal dimension $L_z = 2R/\gamma$ is significantly smaller than the transverse size $2R$, causing the two colliding nuclei to pass each other within a very short timescale L_z/v_z. In this study, we assume

that the electromagnetic fields remain constant during the collisions and are negligible before or after the two nuclei touch, a supposition qualitatively consistent with the findings in Ref. [30].

Following the methodology of STARlight [12, 15, 29, 36], the probability of an UPC event associated with neutron emission ($P_{xn,xn}^{\mathrm{UPC}}$) is calculated as follows:

$$
P_{xn,xn}^{\mathrm{UPC}} = P_{0H}(b) \times P_{xn,xn}(b),
\tag{6}
$$

where $P_{0H}(b)$ denotes the probability of having no hadronic interactions and $P_{xn,xn}(b)$ represents the probability of nuclear breakup with neutron emission in both colliding nuclei [12, 15, 37]. Assuming an independent nuclear breakup, $P_{xn,xn}(b)$ can be factorized as

$$
P_{xn,xn}(b) = P_{xn}(b) \times P_{xn}(b).
\tag{7}
$$

Details of Eqs. (6, 12) can be found in Refs. [12, 15, 29, 36] and in "Appendix."

Mutual Coulomb dissociation is measured at $\sqrt{s_{NN}} = 130$ GeV Au+Au at the RHIC [38]. The measured cross section of "Coulomb"-like events agrees well with the theoretical calculations. The measured neutron multiplicity from a "Coulomb"-like event is concentrated at ~ 1, and at most of ~ 35. Direct measurement of the neutron multiplicity in UPC events is also available for Au + Au collisions at $\sqrt{s_{NN}} = 200$ GeV from the STAR experiment [32, 39], where the neutron multiplicity distribution is comparable to the above result. The Coulomb dissociation of the halo nucleus ^{11}Be at $72A$ MeV [40] shows a $\cos(2\phi)$ modulation between the emitted neutron direction and the impact parameter. A $\cos(2\phi)$ modulation of the neutrons emitted from the two nuclei in the UPC was proposed to estimate the impact parameter direction [41, 42]. The current study primarily focuses on the electromagnetic field impact, which mostly manifests as a back-to-back correlation represented by the $\cos(\phi)$ modulation. The fluctuation of electromagnetic fields that possess both x and y components may induce higher-order $\cos(n\phi)$ modulations. Photoneutron experiments at an energy ~ 20 MeV measured the polar angle of neutron emission, revealing definite anisotropy on Au and Pb targets [43]. Similar results were obtained in other experiments on Coulomb dissociation [40, 44]. Assuming that the photonuclear process is a "direct photoelectric effect", an anisotropic polar angular distribution with a maximum at $\pi/2$ for the neutrons is expected [45]. Nevertheless, because our study primarily focuses on transverse neutron emission, the aforementioned polar angular effect is not considered.

In this study of the neutron emission, the Landau distribution is used to directly estimate the neutron multiplicity from the STAR experiment [32, 39]. As mentioned in Ref. [37], the measurement of spectra for secondary particles from photon–nuclear interactions

is currently limited. Therefore, the neutron energies are generated using the same method as in the $n_{O}^{O}n$ generator [37], utilizing the Evaluated Nuclear Data File (ENDF) tables [46]. ENDF tables for Au are even more limited; tables from ^{208}Pb are currently used. The accuracy could be improved with future measurements; however, this is sufficient for our qualitative study. The energy distribution of the incident photons in a UPC with neutron emission is calculated as [12, 15, 37]

$$
\frac{\mathrm{d}N(k)}{\mathrm{d}k} = \int_0^{+\infty} 2\pi b \mathrm{d}b P_{0H}(b) P_{xn,xn}(b)
$$
$$
\times \int_0^R \frac{r_\perp \mathrm{d}r_\perp}{\pi R^2} \int_0^{2\pi} \mathrm{d}\phi \frac{\mathrm{d}^3 N(k, b + r_\perp \cos(\phi))}{\mathrm{d}k \mathrm{d}^2 r_\perp}. \tag{8}
$$

Neutrons are then produced according to the photon energy and ENDF tables with an isotropic angular distribution [37].

5 Results and discussion

Figure 2 presents the simulation results. The Ψ_n^{east} and Ψ_n^{west} are the first-order harmonic planes [47] constructed by the neutrons emitted from the two nuclei (east and west indicate the two nuclei going opposite directions) in 200 GeV Au + Au UPCs. They are calculated using the sum of the momentum vectors (q vector) [47] of neutrons from each nucleus. Ψ_n^{east} is rotated by π following the experimental conversion. As mentioned in the previous section, the Lorentz force and
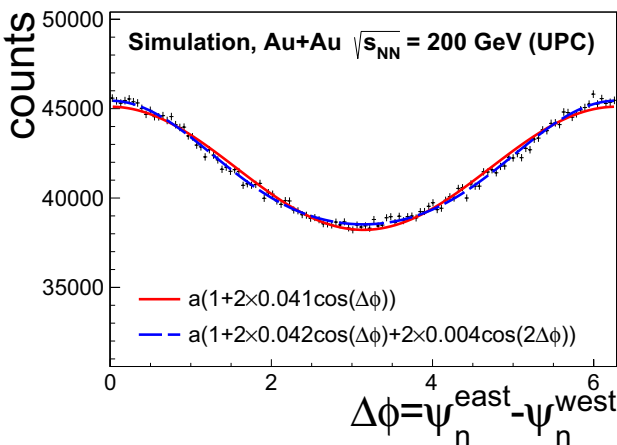
Fig. 2 (Color online) The correlation of the Ψ_n^{east} and Ψ_n^{west} defined by the neutrons emitted from the two colliding nuclei (east and west indicate the two nuclei going opposite directions) in $\sqrt{s_{NN}}$ = 200 GeV Au + Au UPCs. The Ψ_n^{east} is rotated by π following experimental conversion. The red line is a cos (ϕ) fit to the simulated data, which shows that there are strong electromagnetic forces back-to-back to the two colliding nuclei. Due to the fluctuation, the electromagnetic fields have both x and y components. Thus higher-order cos(2ϕ) modulation is also included in the fit, as shown by the dashed line

Coulomb repulsion in such UPCs are sufficiently large to affect the momentum distribution of the emitted neutrons. The red line in Fig. 2 is a cos(ϕ) fit to the simulation, which shows that strong repulsive forces act in opposite directions to the two colliding nuclei. Owing to the fluctuation of electromagnetic fields that possess both x and y components, higher-order cos($n\phi$) modulations may also be present. The dashed line represents a fit that includes the cos(2ϕ)-modulation, which better describes the distribution. Our calculation also demonstrates the sensitivity to the impact parameter direction or the electromagnetic field direction, which could be utilized to study spin-polarization-related physics in UPCs in the future [48–51], as the photons are linearly polarized [21]. This may provide insights into the chiral and spin-related effects in relativistic hadronic heavy-ion collisions, such as CME, hyperon spin polarization, and vector meson spin alignment [7, 52–54].

As discussed in Ref. [11, 41], neutrons have been measured using zero-degree calorimeters (ZDCs) [55] in relativistic heavy-ion collisions. At the RHIC, the ZDCs are positioned ±18 m away from the nominal interaction point at the center of the detector, with dimensions of 10 cm width and 18.75 cm height [55]. For Au + Au collisions at $\sqrt{s_{NN}}$ = 200 GeV at the RHIC, where the neutron longitudinal momentum is $\sim$ 100 GeV, a maximum p_T of 140 MeV/c corresponds to a deflection of approximately 2.5 cm, which is within the acceptance of the ZDCs. With ZDCs' shower-maximum detectors [42], which provide position measurements of neutrons, the measurement of the neutron–neutron correlations between the ZDCs is feasible.

In summary, using Monte Carlo simulation, we demonstrate that the electromagnetic fields generated in UPCs are strong enough to induce measurable back-to-back emission of neutrons in the transverse plane. The effect discussed here provides a clean way for detecting strong electromagnetic fields, as no hadronic interactions are involved, which would be the strongest electromagnetic fields that can be detected to date. It also offers a method to measure the direction of the impact parameter or electromagnetic field. Thus, it may also shed light on chiral and spin-related effects in relativistic hadronic heavy-ion collisions to understand the fundamental features of hot QCD matter. Additionally, this may aid in understanding the initial conditions of hadronic/heavy-ion collisions with a small b, wherein the electromagnetic fields would be considerably stronger.

Appendix

The probability of a UPC event associated with neutron emission ($P_{xn,xn}^{UPC}$) is calculated as follows:

$$
P_{xn,xn}^{UPC} = P_{0H}(b) \times P_{xn,xn}(b), \tag{9}
$$

where $P_{0H}(b)$ denotes the probability of having no hadronic interactions and $P_{xn,xn}(b)$ represents the probability of nuclear breakup with neutron emission in both colliding nuclei [12, 15, 37]. $P_{0H}(b)$ is given by:

$$P_{0H}(b) = \exp[-T_{AA}(b)\sigma_{NN}],$$
$$T_{AA}(b) = \int d^2 r_\perp T_A(r_\perp)T_A(r_\perp - b), \tag{10}$$

where b is the two-dimensional impact parameter vector (with $b = |b|$) in the transverse plane, σ_{NN} is the total nucleon–nucleon interaction cross section, and T_{AA} is the overlap function. The number of nucleon–nucleon collisions follows a Poisson distribution with a mean of $T_{AA}(b)\sigma_{NN}$. The nuclear thickness function T_A is calculated as follows:

$$T_A(r_\perp) = \int dz\, \rho\left(\sqrt{r_\perp^2 + z^2}\right), \tag{11}$$
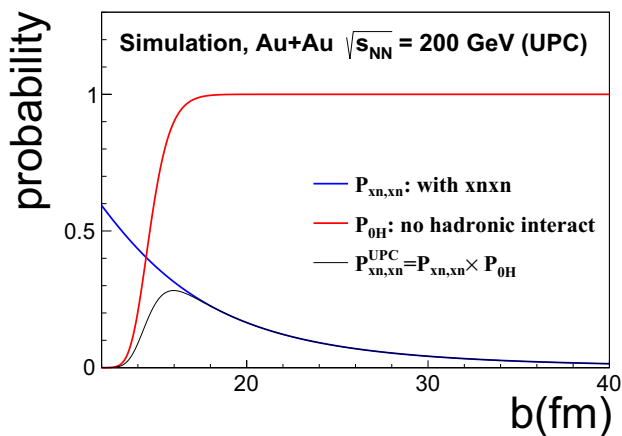
where ρ corresponds to the Woods–Saxon functions in Eq. (4).

Assuming an independent nuclear breakup, $P_{xn,xn}(b)$ can be factorized as

$$P_{xn,xn}(b) = P_{xn}(b) \times P_{xn}(b). \tag{12}$$

Following the methodology of STARlight [12, 15, 29, 36], the probability of nuclear breakup with neutron emission ($P_{xn}(b)$) is given by

$$P_{xn}(b) \propto \int dk \frac{d^3N(b,k)}{dk d^2 b}\sigma_{\gamma A \to A^* + xn}(k), \tag{13}$$

Fig. 3 (Color online) The probability of a UPC event associated with neutron emission ($P_{xn,xn}^{UPC}$, black line), the probability of having no hadronic interactions ($P_{0H}(b)$, red line), and the probability of nuclear breakup with neutron emission in both colliding nuclei ($P_{xn,xn}(b)$, blue line) as a function of the impact parameter in Au+Au collisions at $\sqrt{s_{NN}} = 200$ GeV
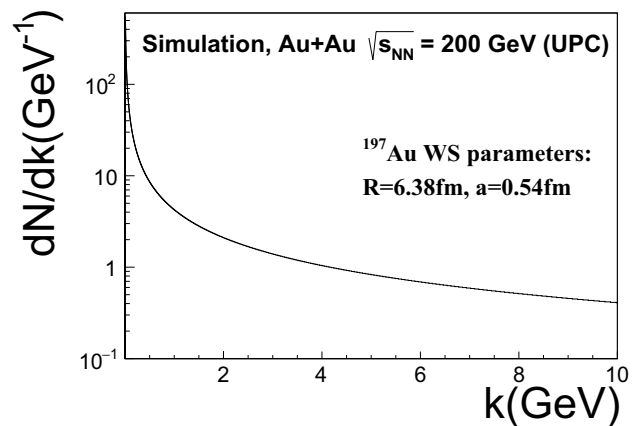
Fig. 4 Photon energy distribution in the target frame in an UPC event with neutron emission using the Weizsäcker–Williams approach with Eqs. (14) and (8)

where $\sigma_{\gamma A \to A^* + xn}$ is determined from experimental data [56, 57]. The photon flux is calculated using the Weizsäcker–Williams approach [12, 15, 58]

$$\frac{d^3N(r_\perp, k)}{dk d^2 r_\perp} = \frac{Z^2 \alpha x^2}{\pi^2 k r_\perp^2}K_1^2(x). \tag{14}$$

where k represents the photon energy, Z is the nuclear charge, K_1 is the modified Bessel function, and $x = kr_\perp/\gamma$. Figure 3 shows $P_{0H}(b)$, $P_{xn,xn}(b)$, $P_{xn,xn}^{UPC}$ obtained from the simulation.

Figure 4 shows the calculation of the photon energy distribution in the target frame for a UPC event with neutron emissions.

Declarations

References

1. D. Kharzeev, R.D. Pisarski, M.H.G. Tytgat, Possibility of spontaneous parity violation in hot QCD. Phys. Rev. Lett. **81**, 512–515 (1998). https://doi.org/10.1103/PhysRevLett.81.512

2. X.G. Huang, Electromagnetic fields and anomalous transports in heavy-ion collisions—a pedagogical review. Rept. Prog. Phys. **79**, 076302 (2016). https://doi.org/10.1088/0034-4885/79/7/076302

3. F.Q. Wang, J. Zhao, Search for the chiral magnetic effect in heavy ion collisions. Nucl. Sci. Tech. **29**, 179 (2018). https://doi.org/10.1007/s41365-018-0520-z

4. J. Zhao, F. Wang, Experimental searches for the chiral magnetic effect in heavy-ion collisions. Prog. Part. Nucl. Phys. **107**, 200–236 (2019). https://doi.org/10.1016/j.ppnp.2019.05.001

5. R. Fang, R. Dong, D. Hou et al., Thermodynamics of the system of massive Dirac fermions in a uniform magnetic field. Chin. Phys. Lett. **38**, 091201 (2021). https://doi.org/10.1088/0256-307X/38/9/091201

6. Y.C. Liu, X.G. Huang, Spin polarization formula for Dirac fermions at local equilibrium. Sci. China Phys. Mech. Astron. **65**, 272011 (2022). https://doi.org/10.1007/s11433-022-1903-8

7. L. Adamczyk, J.K. Adkins, G. Agakishiev et al., Global Λ hyperon polarization in nuclear collisions: evidence for the most vortical fluid. Nature **548**, 62–65 (2017). https://doi.org/10.1038/nature23004

8. J. Adam, L. Adamczyk, M. Zyzak et al., Methods for a blind analysis of isobar data collected by the STAR collaboration. Nucl. Sci. Tech. **32**, 48 (2021). https://doi.org/10.1007/s41365-021-00878-y

9. Y.C. Liu, X.G. Huang, Anomalous chiral transports and spin polarization in heavy-ion collisions. Nucl. Sci. Tech. **31**, 56 (2020). https://doi.org/10.1007/s41365-020-00764-z

10. J.H. Gao, G.L. Ma, S. Pu et al., Recent developments in chiral and spin polarization effects in heavy-ion collisions. Nucl. Sci. Tech. **31**, 9 (2020). https://doi.org/10.1007/s41365-020-00801-x

11. C.A. Bertulani, S.R. Klein, J. Nystrand, Physics of ultra-peripheral nuclear collisions. Ann. Rev. Nucl. Part. Sci. **55**, 271–310 (2005). https://doi.org/10.1146/annurev.nucl.55.090704.151526

12. S.R. Klein, J. Nystrand, J. Seger et al., STARlight: a Monte Carlo simulation program for ultra-peripheral collisions of relativistic ions. Comput. Phys. Commun. **212**, 258–268 (2017). https://doi.org/10.1016/j.cpc.2016.10.016

13. S. Klein, P. Steinberg, Photonuclear and two-photon interactions at high-energy nuclear colliders. Ann. Rev. Nucl. Part. Sci. **70**, 323–354 (2020). https://doi.org/10.1146/annurev-nucl-030320-033923

14. G. Baur, K. Hencken, D. Trautmann, Photon-photon physics in very peripheral collisions of relativistic heavy ions. J. Phys. G **24**, 1657–1692 (1998). https://doi.org/10.1088/0954-3899/24/9/003

15. S. Klein, J. Nystrand, Exclusive vector meson production in relativistic heavy ion collisions. Phys. Rev. C **60**, 014903 (1999). https://doi.org/10.1103/PhysRevC.60.014903

16. C. Adler, Z. Ahammed, C. Allgower et al., Coherent ρ^0 production in ultraperipheral heavy ion collisions. Phys. Rev. Lett. **89**, 272302 (2002). https://doi.org/10.1103/PhysRevLett.89.272302

17. S. Afanasiev, C. Aidala, N.N. Ajitanand et al., Photoproduction of J/ Ψ and of high mass e^+e^- in ultra-peripheral Au+Au collisions at $\sqrt{s_{NN}}$ = 200 GeV. Phys. Lett. B **679**, 321–329 (2009). https://doi.org/10.1016/j.physletb.2009.07.061

18. B. Abelev, J. Adam, D. Adamová et al., Coherent J/ψ photoproduction in ultra-peripheral Pb-Pb collisions at $\sqrt{s_{NN}}$ = 2.76 TeV. Phys. Lett. B **718**, 1273–1283 (2013). https://doi.org/10.1016/j.physletb.2012.11.059

19. V. Khachatryan, et al., Coherent J/ψ photoproduction in ultra-peripheral PbPb collisions at $\sqrt{s_{NN}}$ = 2.76 TeV with the CMS experiment. Phys. Lett. B **772**, 489–511 (2017). https://doi.org/10.1016/j.physletb.2017.07.001

20. M. Aaboud, G. Aad, B. Abbott et al., Evidence for light-by-light scattering in heavy-ion collisions with the ATLAS detector at the LHC. Nat. Phys. **13**, 852–858 (2017). https://doi.org/10.1038/nphys4208

21. J. Adam, L. Adamczyk, J.R. Adams et al., Measurement of e^+e^- momentum and angular distributions from linearly polarized photon collisions. Phys. Rev. Lett. **127**, 052302 (2021). https://doi.org/10.1103/PhysRevLett.127.052302

22. M. Goldhaber, E. Teller, On nuclear dipole vibrations. Phys. Rev. **74**, 1046–1049 (1948). https://doi.org/10.1103/PhysRev.74.1046

23. B.L. Berman, S.C. Fultz, Measurements of the giant dipole resonance with monoenergetic photons. Rev. Mod. Phys. **47**, 713–761 (1975). https://doi.org/10.1103/RevModPhys.47.713

24. P. Chomaz, N. Frascaria, Multiple phonon excitation in nuclei. Phys. Rep. **252**, 275–405 (1995). https://doi.org/10.1016/0370-1573(94)00079-I

25. A. Veyssiere, H. Beil, R. Bergere et al., Photoneutron cross sections of 208 Pb and 197 Au. Nucl. Phys. A **159**, 561–576 (1970). https://doi.org/10.1016/0375-9474(70)90727-X

26. C. Tao, Y.G. Ma, G.Q. Zhang et al., Pygmy and giant dipole resonances by coulomb excitation using a quantum molecular dynamics model. Phys. Rev. C **87**, 014621 (2013). https://doi.org/10.1103/PhysRevC.87.014621

27. W.B. He, Y.G. Ma, X.G. Cao et al., Giant dipole resonance as a fingerprint of α clustering configurations in ^{12}C and ^{16}O. Phys. Rev. Lett. **113**, 032506 (2014). https://doi.org/10.1103/PhysRevLett.113.032506

28. B.S. Huang, Y.G. Ma, Dipole excitation of 6li and 9be studied with an extended quantum molecular dynamics model. Phys. Rev. C **103**, 054318 (2021). https://doi.org/10.1103/PhysRevC.103.054318

29. A.J. Baltz, S.R. Klein, J. Nystrand, Coherent vector meson photoproduction with nuclear breakup in relativistic heavy ion collisions. Phys. Rev. Lett. **89**, 012301 (2002). https://doi.org/10.1103/PhysRevLett.89.012301

30. W.T. Deng, X.G. Huang, Event-by-event generation of electromagnetic fields in heavy-ion collisions. Phys. Rev. C **85**, 044907 (2012). https://doi.org/10.1103/PhysRevC.85.044907

31. A. Bzdak, V. Skokov, Event-by-event fluctuations of magnetic and electric fields in heavy ion collisions. Phys. Lett. B **710**, 171–174 (2012). https://doi.org/10.1016/j.physletb.2012.02.065

32. L. Adamczyk et al., Coherent diffractive photoproduction of ρ^0 mesons on gold nuclei at 200 GeV/nucleon-pair at the Relativistic Heavy Ion Collider. Phys. Rev. C **96**, 054904 (2017). https://doi.org/10.1103/PhysRevC.96.054904

33. J. Chen, D. Keane, Y.G. Ma et al., Antinuclei in heavy-ion collisions. Phys. Rep. **760**, 1–39 (2018). https://doi.org/10.1016/j.physrep.2018.07.002

34. K. Hattori, X.G. Huang, Novel quantum phenomena induced by strong magnetic fields in heavy-ion collisions. Nucl. Sci. Tech. **28**, 26 (2017). https://doi.org/10.1007/s41365-016-0178-3

35. R.D. Woods, D.S. Saxon, Diffuse surface optical model for nucleon-nuclei scattering. Phys. Rev. **95**, 577–578 (1954). https://doi.org/10.1103/PhysRev.95.577

36. A.J. Baltz, Y. Gorbunov, S.R. Klein et al., Two-photon interactions with nuclear breakup in relativistic heavy ion collisions. Phys. Rev. C **80**, 044902 (2009). https://doi.org/10.1103/PhysRevC.80.044902

37. M. Broz, J.G. Contreras, J.D. Tapia Takaki, A generator of forward neutrons for ultra-peripheral collisions: n$_O^O$n. Comput. Phys. Commun. **253**, 107181 (2020). https://doi.org/10.1016/j.cpc.2020.107181

38. M. Chiu, A. Denisov, E. Garcia et al., Measurement of mutual coulomb dissociation in $\sqrt{s_{NN}}$130GeV$au + au$ collisions. Phys. Rev. Lett. **89**, 012302 (2002). https://doi.org/10.1103/PhysRevLett.89.012302

39. B.I. Abelev, M.M. Aggarwal, Z. Ahammed et al., ρ^0 photoproduction in ultraperipheral relativistic heavy ion collisions at $\sqrt{s_{NN}}$ = 200 GeV. Phys. Rev. C **77**, 034910 (2008). https://doi.org/10.1103/PhysRevC.77.034910

40. T. Nakamura, S. Shimoura, T. Kobayashi et al., Coulomb dissociation of a halo nucleus ^{11}Be at 72A MeV. Phys. Lett. B **331**, 296–301 (1994). https://doi.org/10.1016/0370-2693(94)91055-3

41. G. Baur, K. Hencken, A. Aste et al., Multiphoton exchange processes in ultraperipheral relativistic heavy ion collisions. Nucl. Phys. A **729**, 787–808 (2003). https://doi.org/10.1016/j.nuclphysa.2003.09.006

42. STAR ZDCsmd note. https://drupal.star.bnl.gov/STAR/files/ZDC-SMD.pdf

43. F. Tagliabue, J. Goldemberg, Angular distributions of fast photoneutrons. Nucl. Phys. **23**, 144–152 (1961). https://doi.org/10.1016/0029-5582(61)90247-4

44. M. Bakhtiari, N.S. Jung, H.S. Lee, Contribution of compound, preequilibrium and direct reactions to photoneutron emission spectrum from various targets induced by 16.6-MeV monoenergetic photons. Nucl. Instrum. Methods B **521**, 38–46 (2022). https://doi.org/10.1016/j.nimb.2022.03.007

45. E.D. Courant, Direct photodisintegration processes in nuclei. Phys. Rev. **82**, 703–709 (1951). https://doi.org/10.1103/PhysRev.82.703

46. M.B. Chadwick, M. Herman, P. Obložinský et al., ENDF/B-VII.1 nuclear data for science and technology: cross sections, covariances, fission product yields and decay data. Nucl. Data Sheets **112**, 2887–2996 (2011). https://doi.org/10.1016/j.nds.2011.11.002

47. A.M. Poskanzer, S. Voloshin, Methods for analyzing anisotropic flow in relativistic nuclear collisions. Phys. Rev. **58**, 1671–1678 (1998). https://doi.org/10.1103/PhysRevC.58.1671

48. B.W. Xiao, F. Yuan, J. Zhou, Momentum anisotropy of leptons from two photon processes in heavy ion collisions. Phys. Rev. Lett. **125**, 232301 (2020). https://doi.org/10.1103/PhysRevLett.125.232301

49. H. Xing, C. Zhang, J. Zhou et al., The $\cos 2\phi$ azimuthal asymmetry in ρ^0 meson production in ultraperipheral heavy ion collisions. JHEP **10**, 064 (2020). https://doi.org/10.1007/JHEP10(2020)064

50. C. Zhang, Q.S. Dai, D.Y. Shao, Azimuthal decorrelation for photon induced dijet production in ultra-peripheral collisions of heavy ions. JHEP **23**, 002 (2020). arXiv:2211.07071. https://doi.org/10.1007/JHEP02(2023)002

51. X. Wu, X. Li, Z. Tang et al., Reaction plane alignment with linearly polarized photon in heavy-ion collisions. Phys. Rev. Res. **4**, L042048 (2022). https://doi.org/10.1103/PhysRevResearch.4.L042048

52. Z.T. Liang, X.N. Wang, Globally polarized quark-gluon plasma in non-central $A+A$ collisions. Phys. Rev. Lett. **94**, 102301 (2005). [Erratum: Phys.Rev.Lett. 96, 039901 (2006)]. https://doi.org/10.1103/PhysRevLett.94.102301

53. X.N. Wang, Vector meson spin alignment by the strong force field. Nucl. Sci. Tech. **34**, 15 (2023). https://doi.org/10.1007/s41365-023-01166-7

54. J. Chen, Z.T. Liang, Y.G. Ma et al., Global spin alignment of vector mesons and strong force fields in heavy-ion collisions. Sci. Bull. **68**, 874–877 (2023). https://doi.org/10.1016/j.scib.2023.04.001

55. C. Adler, A. Denisov, E. Garcia et al., The RHIC zero degree calorimeter. Nucl. Instrum. Meth. **470**, 488–499 (2001). https://doi.org/10.1016/S0168-9002(01)00627-1

56. A.J. Baltz, M.J. Rhoades-Brown, J. Weneser, Heavy ion partial beam lifetimes due to Coulomb induced processes. Phys. Rev. E **54**, 4233–4239 (1996). https://doi.org/10.1103/PhysRevE.54.4233

57. L.A. Harland-Lang, Exciting ions: a systematic treatment of ultra-peripheral heavy ion collisions with nuclear breakup. Phys. Rev. D **107**, 093004 (2023). arXiv:2303.04826. https://doi.org/10.1103/PhysRevD.107.093004

58. F. Krauss, M. Greiner, G. Soff, Photon and gluon induced processes in relativistic heavy ion collisions. Prog. Part. Nucl. Phys. **39**, 503–564 (1997). https://doi.org/10.1016/S0146-6410(97)00049-5